Pergamon

Geochimica et Cosmochimica Acta, Vol. 66, No. 12, pp. 2273–2285, 2002

0016-7037/02 $22.00 + .00

PII S0016-7037(02)00856-6

Composition of aqueous fluid coexisting with mantle minerals at high pressure and its bearing on the differentiation of the Earth's mantle

KENJI MIBE,*,† TOSHITSUGU FUJII, and ATSUSHI YASUDA

Earthquake Research Institute, University of Tokyo, 1-1-1 Yayoi, Bunkyo-ku, Tokyo 113-0032, Japan

(*Received June* 5, 2001; *accepted in revised form January* 30, 2002)

Abstract—In order to understand the role of aqueous fluid on the differentiation of the mantle, the compositions of aqueous fluids coexisting with mantle minerals were investigated in the system MgO-SiO_2-H_2O at pressures of 3 to 10 GPa and temperatures of 1000 to 1500°C with an MA8-type multianvil apparatus. Phase boundaries between the stability fields of forsterite + aqueous fluid, forsterite + enstatite + aqueous fluid, and enstatite + aqueous fluid were determined by varying the bulk composition at constant temperature and pressure. The composition of aqueous fluid coexisting with forsterite and enstatite can be defined by the intersection of these two phase boundaries. The solubility of silicate components in aqueous fluid coexisting with forsterite and enstatite increases with increasing pressure up to 8 GPa, from about 30 wt% at 3 GPa to about 70 wt% at 8 GPa. It becomes almost constant above 8 GPa. The Mg/Si weight ratio of these aqueous fluids is much higher than at low pressure (0.2 at 1.5 GPa) and almost constant (1.2) at pressures between 3 and 8 GPa. At 10 GPa, it becomes about 1.4. Aqueous fluid migrating upward through the mantle can therefore dissolve large amounts of silicates, leaving modified Mg/Si ratios of residual materials. It is suggested that the chemical stratification of Mg/Si in the Earth may have been formed as a result of aqueous fluid migration. *Copyright © 2002 Elsevier Science Ltd*

1. INTRODUCTION

Aqueous fluid has been considered to play a major role in the differentiation of the mantle, especially through mantle metasomatism and magma generation in subduction zones (e.g., Tatsumi, 1989; Iwamori, 1998). However, the nature of the aqueous fluid in the mantle has not been clarified. Recent experimental studies show there is a drastic change in the connectivity of aqueous fluid in mantle minerals with pressure (Watson and Brenan, 1987; Watson et al., 1990; Mibe et al., 1998; Mibe et al., 1999). The dihedral angles at aqueous fluid–olivine–olivine triple junctions at 1 GPa are too large (~70°) to form an interconnected network of aqueous fluid in polycrystalline olivine (Watson and Brenan, 1987; Watson et al., 1990), indicating that the aqueous fluid in the uppermost mantle cannot segregate at low fluid fraction. In contrast, the dihedral angles in the same system at pressures above 3 GPa are smaller than 50° (Mibe et al., 1998), indicating that an interconnected network of aqueous fluid could be stable. This drastic change in connectivity might imply there could also be drastic compositional changes in aqueous fluids above 3 GPa because in general, dihedral angles show a negative correlation with the solubility of the solid phase into the fluid phase (Takei and Shimizu, 2001).

Nakamura and Kushiro (1974b) showed that aqueous fluid coexisting with forsterite and enstatite contains ~20 wt% SiO_2 at 1.5 GPa and 1280°C (Fig. 1A). Almost no solubility of forsterite component was detected in their experiments. This indicates that the starting composition on the En-H_2O join has an assemblage of either forsterite + enstatite + aqueous fluid (water-poor starting composition) or forsterite + aqueous fluid (water-rich starting composition) at 1.5 GPa. Incongruent dissolution of enstatite was confirmed by Ryabchikov et al. (1982) and Zhang and Frantz (2000). Experiments at higher pressure on the En-H_2O join (Inoue, 1994), however, indicate that only the assemblage of enstatite + vapor is stable above 3 GPa, and no forsterite was observed at subsolidus conditions (Fig. 1B).

Provided that these previous experiments were performed in equilibrium, two possible scenarios are considered: silicate solubility in aqueous fluids becomes almost null at pressures above 3 GPa, or both magnesia and silica become soluble in H_2O—that is, the Mg/Si ratio of aqueous fluid becomes high at pressures above 3 GPa. Taking into account the experimental result that the solubility of quartz in the coexisting aqueous fluid increases with increasing pressure in the system SiO_2-H_2O (e.g., Kennedy et al., 1962; Manning, 1994), aqueous fluid coexisting with mantle minerals at higher pressures may be expected to dissolve larger amounts of silicate including both forsterite and enstatite components. Thus, there is the possibility that aqueous fluid at high pressure dissolves silicate component with Mg/Si ratio larger than unity (in molar ratio).

Luth (1993) discussed the possibility that Mg/Si (molar) ratio of aqueous fluid coexisting with forsterite and hydrous phase E at above 10 GPa was larger than 2. He suggested that this was unlikely, however, and mentioned that the presence of quench clinoenstatite indicates the aqueous fluid to be SiO_2 rich. Also, Luth (1995) reported the assemblage of forsterite + clinoenstatite + aqueous fluid for composition of Mg_2SiO_4 + $2H_2O$ (20.4 wt% H_2O) at pressures between 7 to 10 GPa. Luth (1995) suggested that clinoenstatite may be a quench phase, but he did not mention the aqueous fluid composition. Gasparik (1993) found the presence of aqueous fluid with high Mg/Si ratio in the system MgO-SiO_2-H_2O-MgF_2 at around 17 GPa.

Stalder et al. (2001) determined the composition of aqueous

* Author to whom correspondence should be addressed. (k.mibe@gl.ciw.edu).
† *Present address:* Geophysical Laboratory, Carnegie Institution of Washington, 5251 Broad Branch Rd., NW, Washington, DC 20015.

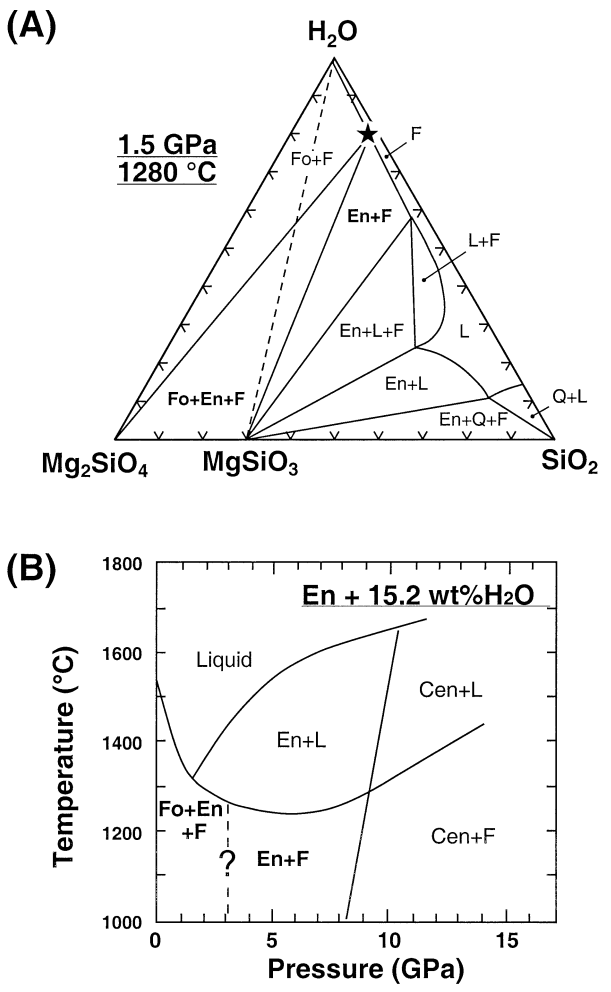

Fig. 1. (A) Isobaric and isothermal section (wt%) of Mg_2SiO_4-SiO_2-H_2O at 1.5 GPa and 1280°C. F = aqueous fluid; Fo = forsterite; En = enstatite. After Nakamura and Kushiro (1974b). Aqueous fluid coexisting with forsterite and enstatite (star) contains ~20 wt% silica. Note that starting composition on the En-H_2O join has an assemblage of either forsterite + enstatite + aqueous fluid (water-poor starting composition) or forsterite + aqueous fluid (water-rich starting composition). (B) Pressure–temperature phase diagram for $MgSiO_3$ + 15.2 wt% H_2O. F = aqueous fluid; L = liquid; Fo = forsterite; En = enstatite; Cen = clinoenstatite. Modified after Inoue (1994). Note that no forsterite is observed at subsolidus condition above 3 GPa.

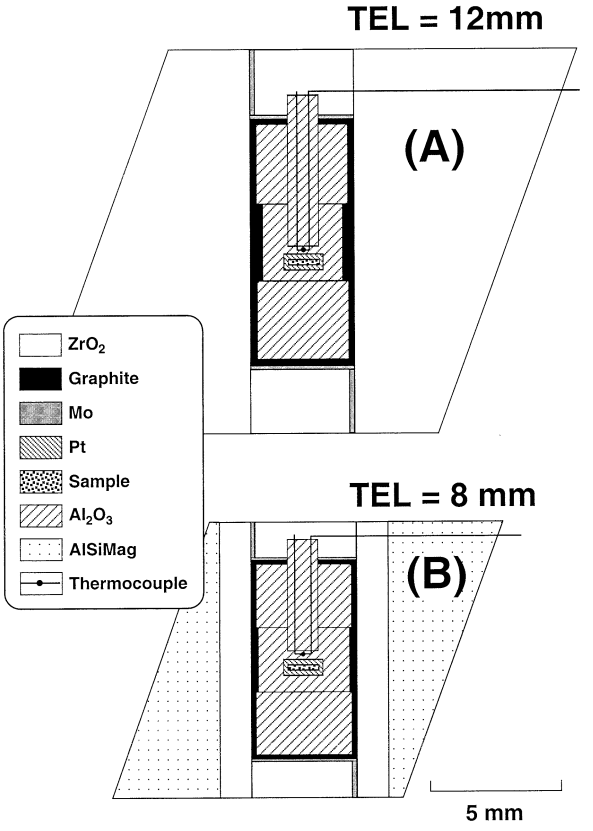

Fig. 2. Schematic diagram showing the furnace assemblies. Scale bar = 5 mm. (A) Assembly for 3 to 6 GPa. (B) Assembly for 8 to 10 GPa. truncated edge length (TEL) is the length of the triangularly truncated corners of tungsten carbide cubes used for the second stage pressurization.

fluid in the system MgO-SiO_2-H_2O at 6.5 to 10.5 GPa and 900 to 1200°C and showed that both the solubility and the Mg/Si ratio increased with pressure. Stalder et al. (2001) used diamond aggregates to trap the fluids and analyzed the recovered diamond traps via laser ablation inductively coupled plasma mass spectrometry. In general, however, aqueous fluid at high pressure cannot be quenched into one phase but into a mixture of glass, quench crystals, and nearly pure water (e.g., Schneider and Eggler, 1986; Mysen and Wheeler, 2000). Therefore, it might be difficult to know the exact compositions of aqueous fluid under the experimental conditions by use of such recovered materials because some quenched materials could be lost preferentially during sample preparation for analysis. Actually, for example, the Mg/Si wt ratio of aqueous fluid that coexisted with enstatite at 9 GPa and 1050°C, using 85 wt% enstatite + 15 wt% H_2O bulk composition (Stalder et al., 2001; run MSH30 in their table 1), is much higher (1.95) than the expected value (0.67).

Instead, phase equilibrium measurements of the run products have been used to determine the composition of unquenchable aqueous fluid phase (e.g., Nakamura, 1974a; Nakamura and Kushiro, 1974b; Ryabchikov et al., 1982; Mysen and Wheeler, 2000; Zhang and Frantz, 2000). In this study, therefore, the compositions of aqueous fluid coexisting with mantle minerals were determined chemographically in the system MgO-SiO_2-H_2O at pressures up to 10 GPa. On the basis of these experimental results, the role of water on the differentiation of the mantle is discussed.

2. EXPERIMENTAL METHODS

2.1. Experimental Procedure

High-pressure experiments were performed with the MA8-type high-pressure apparatus driven by a pair of guide blocks in a uniaxial 2000-ton press (ERI-2000) installed at the Earthquake Research Institute, University of Tokyo. Tungsten carbide (WC) cubic anvils having 12 mm corner truncation edges were used for pressures up to 6 GPa, and anvils with 8-mm truncation were used for pressures up to 10 GPa. Twelve pieces of preformed pyrophyllite gaskets 3.0 mm thick and 6.0 mm wide were used.

The furnace assemblies used in the experiments are shown in Figure 2. A semisintered ZrO_2 octahedron is used as the pressure medium for

experiments with truncated edge length of 12 mm (Fig. 2A). For experiments with truncated edge length of 8 mm, AlSiMag (Technical Ceramics) octahedron is used as the pressure medium (Fig. 2B). A pair of Mo electrodes and a cylindrical graphite heater is used. A cylindrical heater is divided into three cylindrical units (i.e., stepped heater) to reduce the temperature gradient. Temperature gradients of this type of furnace are estimated to be ±10°C/mm at 1100°C from the measurement by Yasuda et al. (1990).

Temperature of the sample was monitored with a W3%Re-W25%Re thermocouple. Because thermocouple emf signals were conducted through the surface of tungsten carbide cubes to the temperature measurement electronics, it was necessary to make a correction for the surface temperature of the anvil. This was done by attaching a chromel–alumel thermocouple to the anvil surface. A correction for the effect of pressure on the thermocouple emf was not applied. The relationship between load and sample pressure was calibrated with the following phase transformations: SiO_2 (quartz–coesite) at 3.2 GPa and 1200°C (Bose and Ganguly, 1995); Fe_2SiO_4 (α to γ) at 5.8 GPa and 1200°C (Yagi et al., 1987); and SiO_2 (coesite–stishovite) at 9.2 GPa and 1200°C and at 10.3 GPa and 1600°C (Zhang et al., 1996). The uncertainties in pressure are estimated to be ±0.3 GPa.

Several starting materials on the join brucite and quartz within the H_2O-Fo-En triangle were prepared to have compositions between forsterite and enstatite on an H_2O-free basis. They are Fo100 + 20.4 wt% H_2O, Fo90En10 + 19.9 wt% H_2O, Fo80En20 + 19.4 wt% H_2O, Fo60En40 + 18.4 wt% H_2O, Fo40En60 + 17.4 wt% H_2O, Fo20En80 + 16.3 wt% H_2O, Fo10En90 + 15.8 wt% H_2O, and En100 + 15.2 wt% H_2O (Fo/En ratio in wt%). Dried powders of $Mg(OH)_2$ (Wako Pure Chemical Industries) and SiO_2 (Soekawa Chemical) were mixed in an agate mortar and pestle under acetone for 1 h, then dried at 120°C for >12 h. These starting materials were loaded into platinum capsules (outer diameter 1.5 mm, inner diameter 1.2 mm) sealed at one end by welding. The capsules were then welded shut to prevent water loss during the experiment.

To investigate the morphology of quench crystals from aqueous fluid and to determine the solubility precisely, one experiment (Fw-20) was conducted with a large amount of water. Solid phases (brucite and quartz) of ~0.65 mg were loaded in a platinum capsule (outer diameter 1.2 mm, inner diameter 1.0 mm, length 8 mm). About 0.11 mg distilled water was added with a microsyringe. The capsule was then welded shut. The amount of water in the capsule was confirmed by weighing the capsule before and after welding. The starting composition of Fw-20 thus prepared was Fo100 + 70 wt%H_2O. The welded capsule was then folded in half, to a length of ~4 mm.

In the experiment, pressure was applied first by loading to the desired pressure, and then temperature was increased to the desired value. The heating duration varied from 1 to 20 h depending on temperature. During experiments, temperature was controlled within ± 3°C of the desired value. After the run, the charge was quenched by means of shutting off the power supply without changing the load. After pressure was released, the sample was recovered.

2.2. Examination of the Run Products

The run products generally consisted of semisintered aggregates of minerals. What existed as fluid-filled porosity at run conditions was preserved upon quench either as void space or as fine-grained quench silicate and glass. Recovered samples were mounted in epoxy and sectioned. The presence of water during the experiments was confirmed by the observation that liquid water was released from the capsule when it was cut after the run. The opened capsule was dried at 120°C for a few hours. Epoxy impregnation and grinding were repeated several times before one side-polished sample was prepared. Although some of the quench crystals and glass may have been lost from the capsule when opened, the presence of quench crystals and glass that remained in the polished sample strongly suggests that aqueous fluid dissolved silicate components under the conditions of the experiments. Chemical analyses of the run products were made with a JEOL 8800R electron microprobe. Typical operating conditions were 15 kV and 1.2×10^{-8} A. In order not to overlook any crystalline phases, some samples that have the critical composition near the phase boundary at experimental conditions were examined more than one section.

Table 1. Experimental conditions and results in the system CaO-MgO-$A1_2O_3$-SiO_2-H_2O.

Run No.	P (GPa)	T (°C)	Duration (h)	Mineral assembly[a]
Pw-30	8	1100	0.5	O1 + Opx + Cpx + Gt + F
Pw-23	8	1100	1	O1 + Opx + Cpx + Gt + F
Pw-13	8	1100	10	O1 + Opx + Cpx + Gt + F
Pw-29	8	1100	30	O1 + Opx + Cpx + Gt + F

[a] O1 = olivine; Opx = orthopyroxine; Cpx = clinopyroxene; Gt = garnet; F = aqueons fluid. Starting composition was SiO_2 38.1 wt%, $Al_2O_3$4.3 wt%, MgO 37.3 wt%, CaO 3.6 wt%, and H_2O 16.7 wt%.

2.3. Chemical Equilibrium and Temperature Gradient

It is important to check whether chemical equilibrium is attained between the aqueous fluid phase and coexisting minerals under high pressure and temperature conditions. To investigate the conditions required to attain chemical equilibrium, a series of experiments in the system CaO-MgO-Al_2O_3-SiO_2-H_2O was conducted before the investigation of phase relations in the system MgO-SiO_2-H_2O. In this system, equilibrium could be evaluated by examining Ca and Al zoning profiles in the minerals.

At 8 GPa and 1100°C, four independent experiments were conducted with durations of 0.5, 1, 10, and 30 h (Table 1). Slight difference in CaO and Al_2O_3 contents between cores and rims of garnet and clinopyroxene were recognized in experiments with rather short durations (0.5 ~ 1 h). After 10 h, the abundances of elements in each mineral reach nearly constant values. Four experiments resulted in the same phase assemblage of olivine + orthopyroxene + clinopyroxene + garnet + aqueous fluid. These results indicate the chemically equilibrated aqueous fluid can be obtained within 10 h at 8 GPa and 1100°C in the system CaO-MgO-Al_2O_3-SiO_2-H_2O. In addition to these, grain sizes obtained are almost the same in the systems both CaO-MgO-Al_2O_3-SiO_2-H_2O and MgO-SiO_2-H_2O under the same conditions. Therefore, 10 h are thought to be enough to obtain chemical equilibrium in the system MgO-SiO_2-H_2O at 1100°C.

Temperature gradients cause segregation differentiation of melt and residual solid by the process that Lesher and Walker (1988) called saturation gradient chemical diffusion, and results in a layered structure (Lesher and Walker, 1988; Walker et al., 1988). Previous melting experiments that used multianvil apparatus were often conducted with large sample capsules (more than a few mm in length). In those cases the temperature gradients were so large that recovered sample consisted of various phase assemblages between the liquidus and the solidus within a single capsule (e.g., Takahashi, 1986; Zhang and Herzberg, 1994). It is very difficult to obtain precise equilibrium phase information from the experiments performed in a capsule with large thermal gradient. To minimize the thermal gradients, Yasuda et al. (1990) have developed stepped heater. In the present study because this kind of segregation differentiation could be enhanced in the system solid and aqueous fluid (e.g., Stalder and Ulmer, 2001), we employed very small platinum capsules with sample height of less than 300 μm in addition to the stepped heater. From Yasuda et al. (1990), temperature gradient within this short capsule is estimated to be less than 10°C. The equilibrium assemblage of forsterite + enstatite + aqueous fluid can be observed like Figure 3(A) in the short capsule. Both forsterite and enstatite are distributed homogeneously in the capsule.

3. RESULTS

3.1. Phase Assemblages

The experimental conditions and the results are shown in Table 2. At temperatures below the solidus, mixtures of feathery, fibrous or needle-like forsterite and enstatite crystals and glass globules of silica were observed in the recovered sample charge (Fig. 3B). All these fine materials are considered to be quench aqueous fluid; that is, they were formed directly from

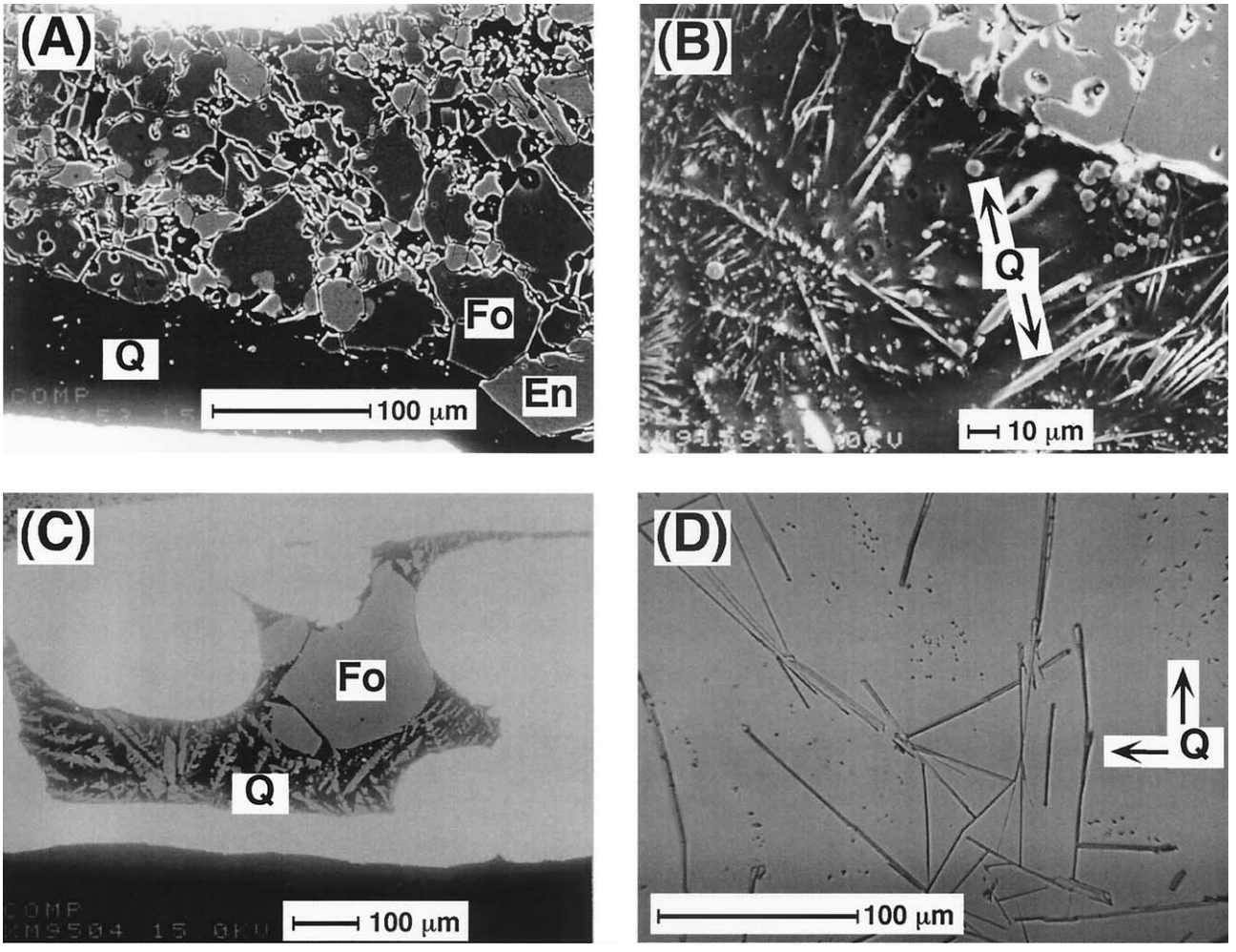

Fig. 3. (A) Forsterite (Fo), enstatite (En), and quenched materials (Q) formed from Fo60En40 + 18 wt% H_2O at 8 GPa and 1100°C (FEw-3). Backscattered electron image. Dark matrix is filled with epoxy. (B) Fo, En, and Q formed from Fo60En40 + 18 wt% H_2O at 8 GPa and 1100°C (FEw-3). Secondary electron image. In this photograph, Fo and En are indistinguishable because contrast of image is optimized to display quench crystals. Dark matrix is filled with epoxy. (C) Fo and Q formed from Fo80En20 + 19 wt% H_2O at 5 GPa and 1300°C (FEw-35). Backscattered electron image. (D) Photomicrograph of Q formed from Fo100 + 70 wt% H_2O at 6 GPa and 1100°C (Fw-20).

the silicate component in the aqueous fluid that existed during the run.

The dissolution of forsterite in aqueous fluid remains congruent up to ~10 GPa at 1100°C. In the system $MgSiO_3$ + 15.2 wt% H_2O, the dissolution of enstatite in aqueous fluid retains its congruent character at pressures between 3 to 8 GPa at 1100°C. On the other hand, at 5 GPa and 1250°C a small amount of forsterite was observed, and the assemblage forsterite + enstatite + aqueous fluid was obtained. This indicates that enstatite dissolution becomes incongruent at 5 GPa and 1250°C. Although we did not determine crystallographic structure of the solid phases, the equilibrium $MgSiO_3$ phase at 10 GPa was estimated to be clinoenstatite from the phase boundary of the orthoenstatite–clinoenstatite transition determined by Pacalo and Gasparik (1990).

3.2. Solidus Temperature in the System MgO-SiO_2-H_2O

In the system SiO_2-H_2O, a second critical end point exists near 1 GPa (e.g., Kennedy et al., 1962). At this point, the univariant solidus curve is terminated (and becomes divariant), and a distinction between aqueous fluid and silicate melt cannot be made. The solidus can be defined only where two fluids coexist. Luth (1993) studied the system MgO-SiO_2-H_2O and noted that the morphology of the quench liquid and quench aqueous fluid remained distinctive to at least 12 GPa. Thus, he concluded that in contrast with the system SiO_2-H_2O, a second critical end point must be at pressures above 12 GPa in the MgO-SiO_2-H_2O system, if present. Stalder et al. (2001) reached the same conclusion.

At 5 GPa, a mixture of feathery crystals and glass coexists with forsterite and enstatite at temperatures between 1000°C and 1200°C for composition of Fo80En20 + 19 wt% H_2O. Enstatite disappears at temperatures between 1250°C and 1275°C, and forsterite is the only crystalline phase. Large quench crystals with the dendritic texture coexist with forsterite at temperatures between 1300°C and 1400°C (Fig. 3C). These dendritic crystals resemble the quench melt obtained in dry melting experiments at high pressures (e.g., Ohtani and Kumazawa, 1981), and in wet melting experiments (Inoue,

Table 2. Experimental conditions and results in the system MgO-SiO_2-H_2O.

Run No.	Starting composition	P (GPa)	T (°C)	Duration (h)	Mineral assembly[a]
FEw-9	Fo90En10	3	1100	9	Fo + En + F
FEw-7	Fo80En20	3	1100	10	Fo + En + F
FEw-8	Fo80En80	3	1100	10	Fo + En + F
Ew-3	En100	3	1100	8	En + F
Fw-12	Fo100	5	1000	77	Fo + F
FEw-15	Fo80En20	5	1000	20	Fo + En + F
FEw-10	Fo90En10	5	1100	8	Fo + F
FEw-11	Fo80En20	5	1100	10	Fo + En + E
FEw-12	Fo20En80	5	1100	10	Fo + En + F
FEw-13	Fo10En90	5	1100	9.5	En + F
Ew-2	En100	5	1100	8	En + F
Ew-5	En100	5	1100	12	En + F
FEw-19	Fo80En20	5	1150	7	Fo + En + F
FEw-48	Fo80En20	5	1150	19	Fo + En + F
FEw-20	Fo80En20	5	1200	5	Fo + F
FEw-47	Fo80En20	5	1200	10	Fo + En + F
Fw-4	Fo100	5	1250	5	Fo + F
FEw-44	Fo90En10	5	1250	5	Fo + F
FEw-34	Fo80En20	5	1250	7	Fo + F
FEw-39	Fo80En20	5	1250	5	Fo + F
FEw-40	Fo60En40	5	1250	5	Fo + En + F
FEw-41	Fo40En60	5	1250	6	Fo + En + F
FEw-42	Fo20En80	5	1250	5	Fo + En + F
FEw-43	Fo10En90	5	1250	5	Fo + En + F
Ew-4	En100	5	1250	5	Fo + En + F
Fw-10	Fo100	5	1275	4	Fo + F
FEw-50	Fo90En10	5	1275	3	Fo + F
FEw-51	Fo80En20	5	1275	3	Fo + F
FEw-52	Fo60En40	5	1275	3	Fo + En + F
Fw-11	Fo100	5	1300	3	Fo + F
FEw-53	Fo90En10	5	1300	3.5	Fo + F
FEw-16	Fo80En20	5	1300	1	Fo + F
FEw-35	Fo80En20	5	1300	2	Fo + L
FEw-54	Fo60Fn40	5	1300	2	Fo + En + L
FEw-55	Fo40En60	5	1300	3	Fo + En + L
FEw-30	Fo80En20	5	1400	1	Fo + L
FEw-17	Fo80En20	5	1500	1.8	L
FEw-36	Fo80En20	5	1500	2	L
Fw-20	Fo100[b]	6	1100	14.5	Fo + F
Fw-1	Fo100	8	1100	10	Fo + F
FEw-2	Fo80En20	8	1100	11.5	Fo + F
FEw-29	Fo80En20	8	1100	12	Fo (+ En)[c] + F
FEw-3	Fo60En40	8	1100	14	Fo + En + F
FEw-4	Fo40En50	8	1100	10	Fo + En + F
FEw-1	Fo20En80	8	1100	10	En + F
Ew-1	En100	8	1100	10	En + F
Fw-3	Fo100	10	1100	12	Fo + F
FEw-22	Fo80En20	10	1100	10	Fo + Cen + F
FEw-27	Fo80En20	10	1100	10	Fo + Cen + F
FEw-33	Fo40En60	10	1100	13.5	Fo + Cen + F
FEw-31	Fo20En80	10	1100	9	Cen + F

[a] Fo = forsterite; En = enstatite; Cen = clinoenstatite; F = aqueous fluid; L = liquid. Starting compositions are represented in weight percent ration of forsterite and enstatite on H_2O-free basis.
[b] Starting composition was Fo + 70 wt% H_2O.
[c] Small amount.

1994; Kawamoto and Holloway, 1997). Thus, they are regarded as quenched hydrous silicate melt.

Therefore, if the two fluids region exists under these conditions as noted in Luth (1993), the solidus in the system forsterite + enstatite + H_2O can be located between 1275°C and 1300°C at 5 GPa. In the same way, from the morphology of the quench crystal, we concluded that 1100°C is subsolidus from 3 to 10 GPa in the system MgO-SiO_2-H_2O.

3.3. Composition of Aqueous Fluid in the System MgO-SiO_2-H_2O

The composition of the aqueous fluid coexisting with forsterite and enstatite was determined chemographically. Direct measurements could not be carried out because the aqueous fluid was quenched into a mixture of feathery crystals, glass and nearly pure water in the recovered sample charge. In the ternary system, if the two fluids region exists, there is an isobaric invariant point where the two fluids coexist with forsterite and enstatite at constant pressure. However, we can observe the assemblage forsterite, enstatite, and quench crystals at several different temperatures and starting compositions at constant pressure. Moreover, because high-pressure silicate liquids in the system MgO-SiO_2-H_2O usually dissolve ~30 wt% H_2O (e.g., Hodges, 1974; Stalder et al., 2001), all experiments reported here can be considered to be slightly water-undersaturated. Although the fluid was not quenched as one homogeneous phase, we can be reasonably certain that it was a single phase (i.e., silicate melt or aqueous fluid) under run conditions. However, on the basis of our results, we cannot decide whether the two fluids region exists or not.

From the phase assemblages obtained in the experiments at constant pressure and temperature with several starting materials having different compositions, we can determine the phase boundary of three regions; forsterite + aqueous fluid, forsterite + enstatite + aqueous fluid, and enstatite + aqueous fluid in the isobaric and isothermal section. Figure 4 shows the isothermal mineral assemblage of Mg_2SiO_4-SiO_2-H_2O at 1100°C and 3 GPa, 5 GPa, 8 GPa and 10 GPa. The shaded regions show the possible compositions of aqueous fluid. Note that because the compositional region of aqueous fluid coexisting with two minerals at constant pressure and temperature in the ternary system must not be a divariant surface but a point in the isobaric and isothermal section, the exact composition of aqueous fluid should be a point within the shaded region.

The aqueous fluids coexisting with forsterite and enstatite contain large amounts of silicate components. The composition of aqueous fluid coexisting with forsterite and enstatite at 3 GPa plots within the subsystem H_2O-Fo-En. Because runs in the subsystem H_2O-Fo-MgO were not performed in the present study, the composition of the aqueous fluid within the triangle H_2O-Fo-En has not been confirmed. It is certain, however, that the Mg/Si ratio of aqueous fluid becomes larger than that of enstatite at 3 GPa and 1100°C. The shift of the composition of aqueous fluid from the region of H_2O-En-silica toward the region of H_2O-En-MgO must occur at pressures between 1 (Zhang and Frantz, 2000) and 3 GPa.

The compositional shift of the aqueous fluid coexisting with mantle minerals with increasing pressure is shown in Figure 5. Also in this figure, the composition of aqueous fluid coexisting with forsterite and enstatite at 1.0 GPa and 1100°C (Zhang and Frantz, 2000) is plotted. Assuming that both solubility and Mg/Si ratio vary monotonically with increasing pressure, the most probable composition of aqueous fluid is estimated at each pressure as shown in Figure 5. The procedures to estimate the most probable composition are as follows:

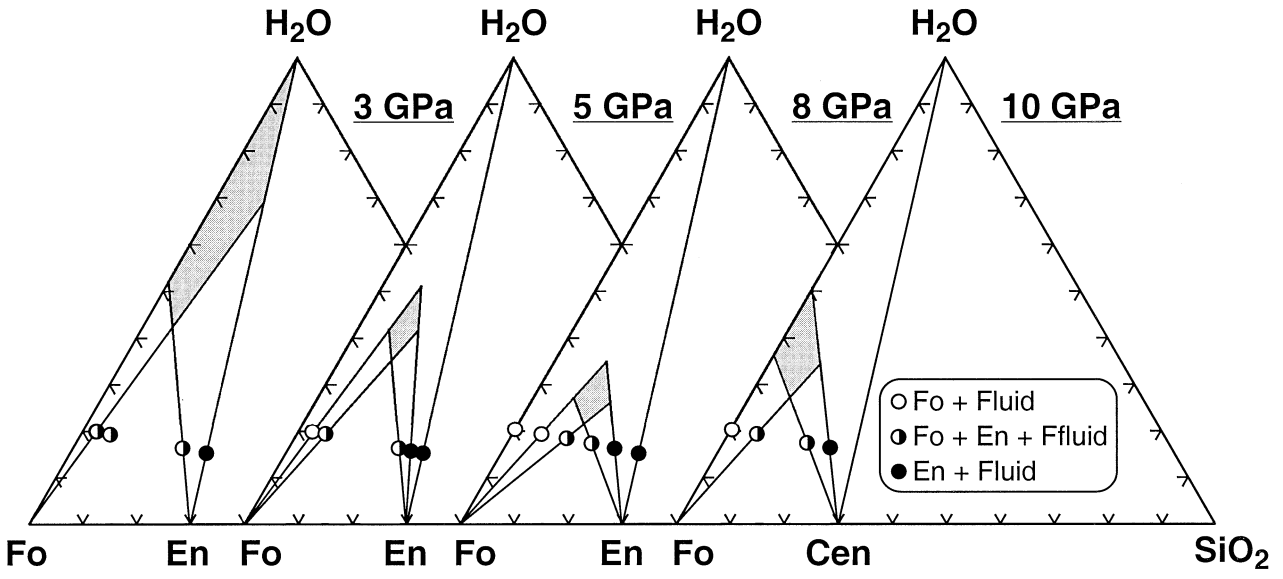

Fig. 4. Composition of aqueous fluid in the system Mg_2SiO_4-SiO_2-H_2O at 1100°C and 3, 5, 8, and 10 GPa. The shaded regions show the possible compositions of aqueous fluid (wt%).

(1) It is assumed that both solubility and Mg/Si ratio increases monotonically with increasing pressure.

(2) From the runs FEw-2 and FEw-29, it is estimated that the starting composition, Fo80En20 + 19.4 wt%H_2O, could be just on the phase boundary between stability fields of forsterite + aqueous fluid and forsterite + enstatite + aqueous fluid at 8 GPa and 1100°C. Therefore, the composition of aqueous fluid at 8 GPa is most likely to be in the upper left side of the rhombic and shaded area at 8 GPa.

(3) From the above constraints 1 and 2, the most probable compositions of aqueous fluid at 8 and 10 GPa are determined as shown in Figure 5.

(4) The points at 1 GPa by Zhang and Frantz (2000) and ours at 8 GPa are joined by a smooth curve. The middle points, where the smooth curve passes through the rhombic and shaded areas at 3 and 5 GPa, are considered to be the most probable composition of aqueous fluid at 3 and 5 GPa, respectively.

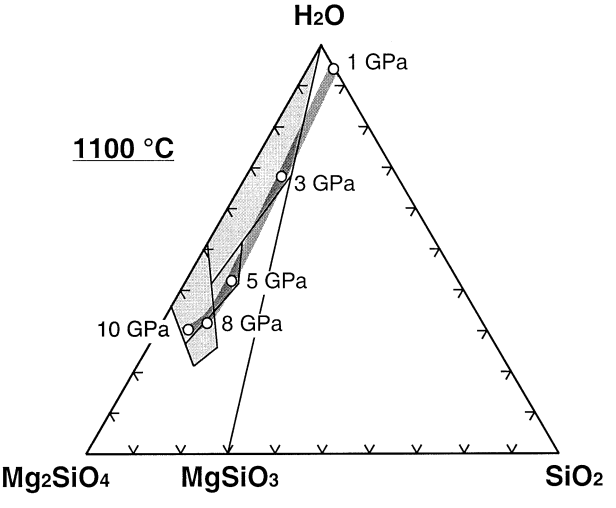

Fig. 5. Pressure effect on composition of aqueous fluid in the system Mg_2SiO_4-SiO_2-H_2O at 1100°C. Numbers indicate pressures. The shaded regions show the possible compositions of aqueous fluid from Figure 4. Data at 1 GPa and 1100°C from Zhang and Frantz (2000).

Solubility of silicate components in aqueous fluid coexisting with forsterite and enstatite increases with increasing the pressure up to 8 GPa; from ~30 wt% at 3 GPa to 70 wt% at 8 GPa. It becomes almost constant above 8 GPa. The aqueous fluid coexisting with forsterite and clinoenstatite at 10 GPa also contains ~70 wt% silicate components. The Mg/Si wt ratio of aqueous fluid is almost constant (1.2) at pressures between 3 to 8 GPa. At 10 GPa, it increases to ~1.4.

To confirm the high silicate solubility and morphology of quench crystals at high pressure, we conducted one experiment with a large amount of water (Fw-20). The total amount of water added was ~70 wt%. By use of this starting composition, we intended to have obtained a sample in which aqueous fluid only was stable at experimental conditions.

Most of materials in the recovered capsule consisted of quench crystals from aqueous fluid (Fig. 3D). The texture of quench fluid in Fig. 3D is definitely different from that of hydrous silicate melts by Inoue (1994) and Kawamoto and Holloway (1997). However, a small amount of forsterite was observed in the coldest end of the capsule. This could suggest that the solubility of forsterite on the Fo-H_2O join was less than 30 wt% at 6 GPa and 1100°C. However, the temperature gradient within this large capsule (~4 mm length) could be large. In addition to this, it was difficult to estimate the forsterite/aqueous fluid ratio in the recovered capsule. Therefore, the solubility of forsterite unfortunately could not be determined from the run Fw-20.

3.4. Effect of Temperature on the Composition of Aqueous Fluid

At 5 GPa and 1250°C, an assemblage of forsterite + enstatite + aqueous fluid was observed for the starting composition of

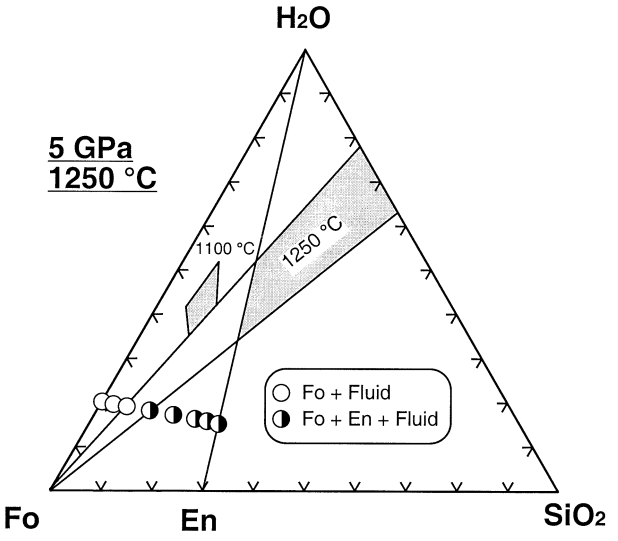

Fig. 6. Temperature effect on composition of aqueous fluid in the system Mg_2SiO_4-SiO_2-H_2O at 1250°C and 5 GPa. Data at 1100°C from Figure 4B.

$MgSiO_3$ + 15.2 wt% H_2O. In other words, enstatite was dissolved in the aqueous fluid in an incongruent manner, and the aqueous fluid coexisting with forsterite and enstatite is in the region of H_2O-En-silica.

Figure 6 shows an isothermal section of Mg_2SiO_4-$MgSiO_3$-H_2O at 5 GPa and 1250°C. The shaded region denoted by 1250°C shows the possible composition of the aqueous fluid. The composition of aqueous fluid at 5 GPa and 1100°C from Figure 4 is also shown as the shaded region (denoted by 1100°C). Because the experiment with starting composition in the region of H_2O-En-silica was not conducted, the composition of aqueous fluid at 5 GPa and 1250°C is not well constrained. However, it should be noted that the composition of aqueous fluid coexisting with forsterite and enstatite shifts from the region of H_2O-Fo-En toward that of H_2O-En-silica with increasing temperature from 1100°C to 1250°C. This suggests that the aqueous fluid coexisting with forsterite and enstatite becomes increasingly silica rich with increasing temperature.

3.5. Estimation of Phase Diagram in the System MgO-SiO_2-H_2O

From all the experimental results listed in Table 2, isobaric (5 GPa) and isothermal sections of Mg_2SiO_4-SiO_2-H_2O are constructed (Fig. 7). As described above, because we cannot determine whether two fluids region exists in the present study, two possible sections are proposed at 1290°C (Fig. 7, C1 vs. C2) and 1300°C (Fig. 7, D1 vs. D2). Figures 7C1 and D1, show the sections in the case a two-fluid region exists, whereas, Figures 7C2 and D2 show them in the case it does not exist. In the latter case, although the fluid phases having relatively H_2O rich (at low temperature) and H_2O-poor (at high temperature) composition are denoted as F and L, respectively, the fluid changes continuously from one to another. Because we can only determine the equilibrium mineral assemblages and the composition of one fluid phase coexisting with two minerals in the present study, Figure 7 represents only topological solutions. The actual locations of aqueous fluids and silicate melts are still to be fully determined.

If a two-fluid region exists, run products of FEw-16, 35, and 53 are the most likely candidates for two coexisting fluids with forsterite. However, we cannot observe the texture of phase separation or the spherical quenching texture peculiar to the system that has an immiscible fluids field; for example, in the system Fe-FeO (e.g., Ohtani and Ringwood, 1984). There may be some explanations for this. One is that there is little difference of the surface tension between silicate melt and aqueous fluid, because the physical nature of hydrous melt and silicate-rich aqueous fluid becomes closer with increasing pressure. Another possibility is that all experiments in the present study are water-undersaturated, as discussed in section 3.3.

Figure 8A, B show the pseudo binary phase diagram on the join $MgSiO_3$-H_2O at 5 GPa. Figure 8A shows the diagram in the case that a two-fluid region exists, whereas Figure 8B shows the case when a two-fluid region does not exist. In both cases, the field of enstatite + aqueous fluid transforms to forsterite + enstatite + aqueous fluid with increasing temperature because the composition of aqueous fluid shifts from the region Mg_2SiO_4-$MgSiO_3$-H_2O to the region $MgSiO_3$-SiO_2-H_2O with increasing temperature. The field of forsterite + aqueous fluid appears on the H_2O-rich side accompanied by the compositional shift of aqueous fluid described above. From the fact that enstatite melts congruently under the dry condition at 5 GPa (e.g., Kato and Kumazawa, 1985), there must be a range of H_2O content beyond anhydrous conditions where forsterite disappears before enstatite with increasing temperature (see dotted lines in Fig. 8).

4. DISCUSSION

4.1. Comparison with Previous Studies on Aqueous Fluid Composition

Ryabchikov et al. (1982) reported the compositions of the aqueous fluid coexisting with forsterite and enstatite in the system Mg_2SiO_4-SiO_2-H_2O at 3 GPa. Although the Mg/Si ratio of aqueous fluid at 3 GPa and 1100°C is larger than that of enstatite in the present study, their result shows that the composition of aqueous fluid at 3 GPa and 1100°C is in the region of H_2O-En-silica. Kushiro et al. (1968) also conducted experiments on the join En-H_2O at 3 GPa and 1100°C and obtained an assemblage of forsterite, enstatite, and aqueous fluid, suggesting that the fluid composition at this pressure and temperature should also be in the region of H_2O-En-silica rather than in the region of H_2O-Fo-En.

Solubility of silicate components in aqueous fluid at 3 GPa and 1100°C has been poorly constrained in the present study. This is because the composition of aqueous fluid at 3 GPa is likely to be located far from the starting compositions used. In general, the smaller the compositional differences between the aqueous fluid at high pressure and the starting materials, the more precisely we can determine the composition of fluid phase by the phase equilibrium measurements. However, it is difficult to prepare the starting materials having water content more than the mixtures of $Mg(OH)_2$ and SiO_2 because of the difficulty in enclosing small amount of water accurately with the very small sample capsules used in the present study. It cannot be denied

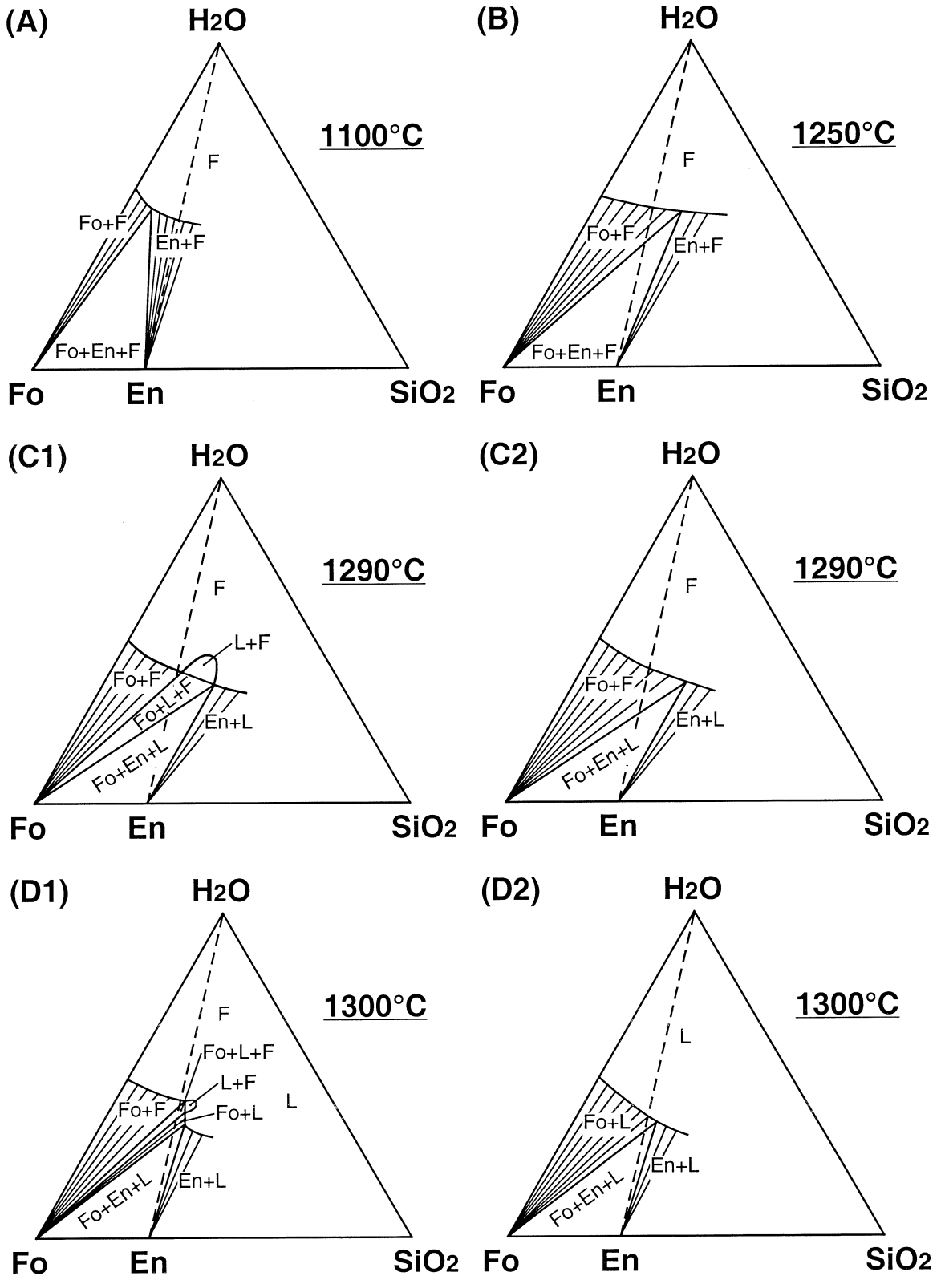

Fig. 7. Isobaric and isothermal sections at 5 GPa and (A) 1100°C, (B) 1250°C, (C1) and (C2) 1290°C, and (D1) and (D2) 1300°C. (C1) and (D1) show the sections in the case two-fluid region exists. (C2) and (D2) show the sections in the case two-fluid region does not exist.

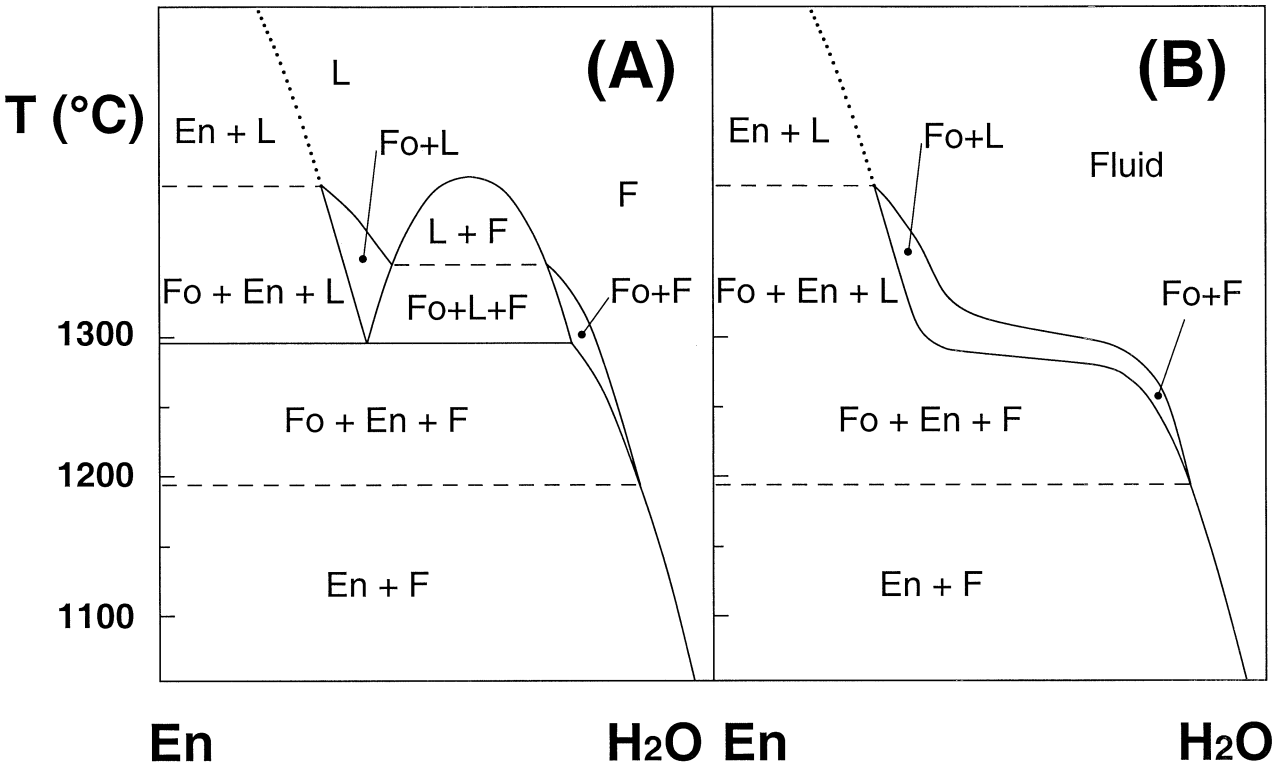

Fig. 8. Pseudo binary phase diagram on the join $MgSiO_3$-H_2O at 5 GPa. (A) Diagram in the case when a two-fluid region exists. (B) Diagram in the case when a two-fluid region does not exist. Because the liquidus phase relations in H_2O-undersaturated compositions were not determined precisely, the fields of En + L were drawn by dotted lines.

that the overlook of a small amount of forsterite in the run Ew-3 might have caused the compositional difference between the results of the present study and those by Ryabchikov et al. (1982) and Kushiro et al. (1968). This is because the run Ew-3 only is the constraint to determine whether the Mg/Si ratio of aqueous fluid at 3 GPa is higher than that of enstatite or not.

Previous experimental results on the composition of aqueous fluid in the system MgO-SiO_2-H_2O at pressures less than 3 GPa show the composition of aqueous fluid coexisting with forsterite and enstatite is in the region of H_2O-En-silica. Nakamura and Kushiro (1974b) (Fig. 1A) showed that aqueous fluid coexisting with forsterite and enstatite contained ~20 wt% silica at 1.5 GPa. The SiO_2 content of the aqueous fluid coexisting with forsterite and enstatite increased with increasing temperature and reached a maximum at 1315°C, where the melting begins. Almost no solubility of forsterite component was detected in their experiments. This conclusion was confirmed by Zhang and Frantz (2000), who provided more systematic results in the MgO-SiO_2-H_2O in the 1.0- to 2.0-GPa and 900 to 1200°C pressure and temperature range, respectively.

At higher pressures (up to 7.7 GPa), Yamamoto and Akimoto (1977) reported that the dissolution of enstatite into aqueous fluid retained its congruent character even at high temperature (1225°C at 7.2 GPa), suggesting that the aqueous fluid composition coexisting with forsterite and enstatite should be in the region of H_2O-Fo-En rather than in the region of H_2O-En-silica. Inoue (1994) also obtained the assemblage of enstatite + aqueous fluid above 5 GPa at 1100°C on the join En-H_2O (Fig. 1B). Therefore, although the reason for the compositional discrepancy between the results of the present study and those obtained by Ryabchikov et al. (1982) and Kushiro et al. (1968) is not clear, the shift of the composition of aqueous fluid coexisting with forsterite and enstatite at 1100°C from H_2O-En-silica toward H_2O-Fo-En does occur at least at pressures between 3 and 5 GPa as shown in Figure 5.

Stalder et al. (2001) also reported compositions of aqueous fluids in the system MgO-SiO_2-H_2O at 6 to 10.5 GPa and 900 to 1200°C. The silicate solubility reported in Stalder et al. (2001) is much smaller than our results by approximately 50% at the same P-T conditions. Stalder et al. (2001) used diamond aggregates to trap dissolved material precipitated after quenching. So, their fluid may not be the pure H_2O but the C (diamond)-saturated C-H-O fluid. Although Stalder et al. (2001) determined the mole fraction of H_2O in the quenched fluid to be >0.99 by gas chromatography, quenched fluid may not preserve the composition that the fluid had under high pressure and temperature conditions. For example, it is reported that carbonate was precipitated from the C-H-O fluid after quenching in the system MgO-SiO_2-H_2O-CO_2 (Eggler et al., 1979) and in the peridotite-H_2O-CO_2 system (Mysen and Boettcher, 1975). Therefore, the difference of the solubility between Stalder et al. (2001) and the present study could be explained by the compositional difference of the C-H-O fluid.

4.2. Aqueous Fluid in Natural vs. MgO-SiO_2-H_2O System

The applicability of phase relations and aqueous fluid composition in a simplified model system to the natural mantle

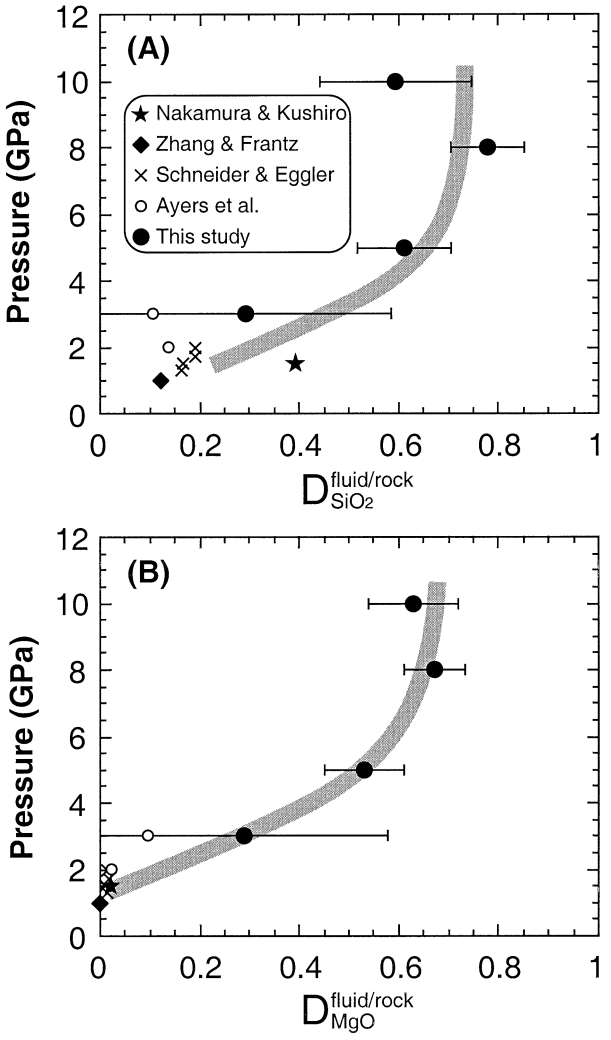

Fig. 9. Pressure dependence of the bulk partition coefficients for aqueous fluid/peridotite. The bars denote the range of the partition coefficients that depend on the ranges of restricted composition of aqueous fluid obtained in our experiments (shaded region in Fig. 4). Solid circles are intermediate values of each range at each pressure. The shaded line is drawn to be consisted with the curve in Figure 5. Bulk partition coefficients by Nakamura and Kushiro (1974b), Zhang and Frantz (2000), and the present study are in the MgO-SiO_2-H_2O system, and those by Schneider and Eggler (1986) and Ayers et al. (1997) are in a natural system.

process may be questioned on grounds that important components of Earth's mantle such as FeO, CaO, and Al_2O_3 are missing. Before proceeding to some applications to the Earth, therefore, the issue of relevance will be addressed.

The pressure dependence of the bulk partition coefficients for aqueous fluid/peridotite is shown in Figure 9. The peridotite having the composition of Fo70En30 is adopted as an approximation of mantle rock in the calculations. Bulk partition coefficients by Nakamura and Kushiro (1974b) and Zhang and Frantz (2000) in the MgO-SiO_2-H_2O system and those by Schneider and Eggler (1986) and Ayers et al. (1997) in a natural system are also plotted in Figure 9. The shaded line is drawn to be consistent with the curve in Figure 5.

Partition coefficients of SiO_2 in the natural system studied by Schneider and Eggler (1986) are obtained at nearly isothermal conditions (1.3 ~ 1.7 GPa at 1080°C; 2.0 GPa at 1100°C), and increase with increasing pressure as seen in the MgO-SiO_2-H_2O system. The correlation between temperature and partition coefficient of SiO_2 is expected to be positive from our experimental results (shown in Fig. 6). This tendency can also be seen in the natural system; the partition coefficient at 3 GPa and 800°C by Ayers et al. (1997) is smaller than that at 2 GPa and 1100°C. Partition coefficients of MgO in the natural system studied by Schneider and Eggler (1986) also increase slightly with increasing pressure. The value by Ayers et al. (1997) becomes large at 3.0 GPa. Their results are very much consistent with the present study in the MgO-SiO_2-H_2O system.

The applicability of our simple system data to natural mantle is also justified in the light of dissolution reactions. The composition of aqueous fluid at pressures between 1 and 2 GPa in the MgO-SiO_2-H_2O system (Nakamura and Kushiro, 1974b; Zhang and Frantz, 2000) is in the region of H_2O-En-silica. This indicates that incongruent dissolution of enstatite occurs at this comparative low pressure, leaving an olivine residuum. Schneider and Eggler (1986) also reported the incongruent dissolution of enstatite up to 2 GPa in natural system. On the other hand, our simple-system results show that enstatite dissolves congruently above 3 GPa. The approximate mass balance calculation on Mg-rich aqueous fluid observed in the natural system at 3 GPa by Ayers et al. (1997) also indicates that congruent dissolution of enstatite, olivine, and garnet occurs. Therefore, not only are the P-T dependence of partition coefficients in MgO-SiO_2-H_2O system similar to those in the natural system, but the change of dissolution reactions with pressure is also similar, indicating that phase relations and fluid compositions in MgO-SiO_2-H_2O system are a good guide to those in natural peridotite.

5. IMPLICATIONS FOR THE EARTH'S DIFFERENTIATION

5.1. Differentiation of the Mantle

According to Mibe et al. (1998), aqueous fluid in the upper mantle can migrate upward by percolation because the dihedral angle at aqueous fluid–forsterite–forsterite triple junction is less than 60° at high pressure and temperature. Aqueous fluid migrating upward through the mantle can dissolve large amounts of silicate components leaving modified Mg/Si ratios of residual rocks. This process could result in differentiation of originally homogeneous Earth's mantle as suggested by Fujii et al. (1996), Mibe et al. (1997), and Stalder et al. (2001).

The estimated Mg/Si ratio of the Earth's upper mantle ranges from ~0.98 to 1.1 (e.g., Ringwood, 1966; Green et al., 1979; Jagoutz et al., 1979; Palme and Nickel, 1985) and is higher than that of chondritic meteorites (0.93: Wasson and Kallemeyn, 1988; Anders and Grevesse, 1989). The difference of Mg/Si ratio between upper mantle and primitive chondrites has been attributed to fractionation of $MgSiO_3$ perovskite (e.g., Kumazawa, 1981; Ohtani, 1985) or majorite garnet (e.g., Ohtani et al., 1986; Herzberg and Gasparik, 1991) in a deep magma ocean during the early stage of the Earth. However, experimental studies on element partitioning (e.g., Kato et al., 1988a; Kato et al., 1988b; McFalane et al., 1994; Gasparik and Drake, 1995) have revealed that significant separation of high

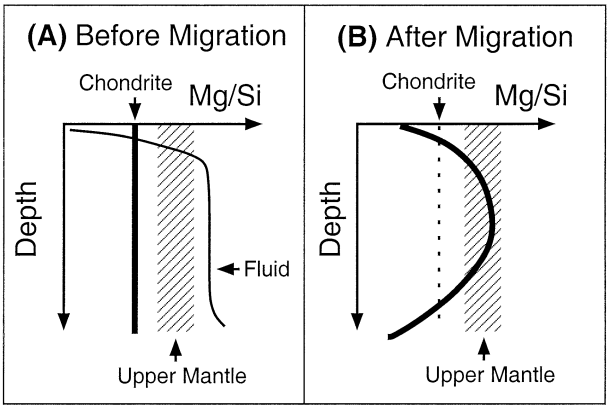

Fig. 10. Mg/Si ratio of the mantle (thick line) before (A) and after (B) migration of aqueous fluid. Thin line represents the composition of aqueous fluid coexisting with forsterite and enstatite. Shaded region shows the compositional range of present upper mantle. Mg/Si ratio of chondrite is also indicated and is smaller than that of present upper mantle. Aqueous fluid migrating upward through the mantle can dissolve a large amount of silicates, leaving modified Mg/Si ratios of residual materials. The deeper part becomes Si rich as a result of releasing high Mg/Si component, whereas the shallower part becomes Mg rich. The surface region becomes Si rich again because low-Mg/Si ratio aqueous fluid (Nakamura and Kushiro, 1974b; Zhang and Frantz, 2000) is supplied.

pressure minerals also results in fractionation of several element pairs away from chondritic ratios, which the primitive mantle is supposed to retain.

Instead of fractional crystallization differentiation in the deep magma ocean, another explanation (Fig. 10) for producing the Mg/Si contrast in the mantle is as follows. As shown in section 3.3, aqueous fluids coexisting with mantle minerals have higher Mg/Si ratio ($>$1.2 above 3 GPa) than the primitive chondrites (0.93), and the solubility of silicate component increases with increasing pressure. Therefore, segregation of aqueous fluid from mantle materials may cause differentiation of mantle material in terms of Mg/Si component. In the deep mantle, the composition of residual solid becomes Si rich as a result of releasing high Mg/Si aqueous fluid. On the other hand, shallower mantle becomes Mg rich as a result of precipitating the high Mg/Si component owing to the difference of solubility with pressure. This region may correspond to the present upper mantle. At the shallowest depths, Si-rich region is formed again because significantly Si-rich aqueous fluid (Nakamura and Kushiro, 1974b; Zhang and Frantz, 2000) is supplied.

Is the migration of aqueous fluid quantitatively effective in modifying the Mg/Si ratio of the Earth's interior? A simple mass balance calculation of the migration and precipitation of aqueous fluid from the lower mantle to the upper mantle that uses the composition of aqueous fluid at 10 GPa (Mg/Si wt ratio = 1.4) reveals that the transfer of aqueous fluid with the mass fraction of only 6.6 wt% of the lower mantle can explain the increase of the Mg/Si ratio of the upper mantle from the chondritic value (0.93) to the present one (0.98). The H_2O content of this aqueous fluid removed from the lower mantle corresponds to 2.0 wt% of the mass of the lower mantle before migration. In the calculation, the aqueous fluid of the composition at 10 GPa was assumed to precipitate all the silicate components in the upper mantle. Carbonaceous chondrites contain up to 20 wt% H_2O (Wiik, 1956) and according to two-component model, ~10% of the source materials of the Earth is thought to be composed of carbonaceous chondrite-like materials (e.g., Ringwood, 1977; Dreibus and Wänke, 1987). Therefore, the removal of 2.0 wt% H_2O (that is, 6.6 wt% aqueous fluid) could be probable, because average water content of the Earth-forming source materials might be a few weight percent. Heterogeneous Mg/Si in the mantle therefore can be formed without fractional crystallization in the deep molten magma ocean. It is important to note that the chemical differentiation by the aqueous fluid migration is not in conflict with the magma ocean model. This is because the migration of aqueous fluid in the mantle could have occurred not only in the cold accreting Earth but also by the proceeding solidification of the hydrous magma ocean.

5.2. Origin of the Continental Crust

The existence of a chemically evolved (broadly andesitic; ~60 wt% SiO_2) continental crust is one of the unique features of the Earth when compared with other terrestrial planets in the solar system (Taylor and McLennan, 1985). Most models of crustal formation require complex multistage melting processes to derive the evolved feature of the continental crust from the mantle with ultramafic composition (e.g., review in Rudnick, 1995).

Kelemen (1995) suggested that it might be possible to form the continental crust in a single stage melting process, because the compositions of the low-degree partial melts of anhydrous mantle peridotite are andesitic (Baker et al., 1995). However, the high viscosities of these melts (Baker et al., 1995) make it difficult to produce volumetrically significant andesite (Rudnick, 1995). Moreover, Falloon et al. (1997) insisted that the composition of low-degree mantle melts are not andesitic but nepheline normative (Na_2O rich) under dry conditions, and raised a doubt about the results of Baker et al. (1995).

Our new scenario for differentiating the mantle is also a possible mechanism for making the continental crust. Migrating aqueous fluid, which had already modified the Mg/Si ratio of the mantle, would finally precipitate the Si-rich component at the shallowest part because the composition of aqueous fluid becomes Si rich and solubility becomes small at low pressure (Nakamura and Kushiro, 1974b; Zhang and Frantz, 2000). Thus, a silica-rich zone or pyroxene veins would have formed in the relatively shallower portion of the mantle peridotite because there would be a transition zone between large-scale channeled and porous flow regimes due to the pressure and temperature dependence of the connectivity of aqueous fluid in mantle minerals (Watson et al., 1990; Mibe et al., 1998; Mibe et al., 1999).

When melting of such a silica-rich zone or pyroxene veins among peridotite occurred, silicic magma may have been formed and extruded on the Earth's surface to generate the protocontinental crust. Because magmas formed from vein plus wall rock melting mechanisms (Foley, 1992) are hybrids in all portions of melt components derived from melting of veins (felsic magma) and by melting of surrounding wall rocks (mafic magma), andesitic magma could be formed by a single stage melting of such a mantle peridotite. The continental crust

thus originated might have grown mainly by the addition of andesites in subduction zones (e.g., Taylor, 1967).

Acknowledgments—We thank T. Sano, D. Yamazaki, K. Kaneko, S. Ono, T. Hanyu, and T. Kawamoto for their helpful comments, discussions, and encouragement. We are grateful to I. Kaneoka, T. Koyaguchi, S. Nakada, and Y. Miura for their advice and discussions. J. A. Van Orman, G. H. Gudfinnsson, and Y. Fei are thanked for helping us to improve the manuscript. We also thank C. Manning and two anonymous reviewers for their critical and constructive reviews. Prepared with support from the Research Fellowships of the Japan Society for the Promotion of Science for Young Scientists.

Associate editor: B. Mysen

REFERENCES

Anders E. and Grevesse N. (1989) Abundances of the elements: Meteoritic and solar. *Geochim Cosmochim Acta* **53,** 197–214.

Ayers J. C., Dittmer S. K., and Layne G. D. (1997) Partitioning of elements between peridotite and H_2O at 2.0–3.0 GPa and 900–1100°C, and application to models of subduction zone processes. *Earth Planet Sci Lett* **150,** 381–398.

Baker M. B., Hirschmann M. M., Ghiorso M. S., and Stolper E. M. (1995) Compositions of near-solidus peridotite melts from experiments and thermodynamic calculations. *Nature* **375,** 308–311.

Bose K. and Ganguly J. (1995) Quartz–coesite transition revisited: Reversed experimental determination at 500–1200°C and retrieved thermochemical properties. *Am. Mineral.* **80,** 231–238.

Dreibus G. and Wänke H. (1987) Volatiles on Earth and Mars: A comparison. *Icarus* **71,** 225–240.

Eggler D., Kushiro I., and Holloway J. (1979) Free energies of decarbonation reactions at mantle pressures: I. Stability of the assemblage forsterite–enstatite–magnesite in the system MgO-SiO_2-CO_2-H_2O to 60 kbar. *Am. Mineral.* **64,** 288–293.

Falloon T. J., Green D. H., O'Neill H. St. C., and Hibberson W. O. (1997) Experimental tests of low degree peridotite partial melt compositions: Implications for the nature of anhydrous near-solidus peridotite melt at 1 GPa. *Earth Planet Sci Lett* **152,** 149–162.

Foley S. (1992) Vein-plus-wall-rock melting mechanisms in the lithosphere and the origin of potassic alkaline magmas. *Lithos* **28,** 435–453.

Fujii T., Mibe K., and Yasuda A. (1996) Composition of fluid coexisting with olivine and pyroxene at high pressure: The role of water on the differentiation of the mantle (abstract). *Misasa Seminar on Evolutionary Processes of Earth and Planetary Materials*, 37–38.

Gasparik T. (1993) The role of volatiles in the transition zone. *J Geophys Res* **98,** 4287–4299.

Gasparik T. and Drake M. J. (1995) Partitioning of elements among two silicate perovskites, superphase B, and volatile-bearing melt at 23 GPa and 1500–1600°C. *Earth Planet Sci Lett* **134,** 307–318.

Green D. H., Hibberson W. O., and Jaques A. L. (1979) Petrogenesis of mid–ocean ridge basalts. In *The Earth: Its Origin Structure and Evolution* (ed. MW McElhinny), 265–290. Academic Press.

Herzberg C. T. and Gasparik T. (1991) Garnet and pyroxene in the mantle: A test of the majorite fractionation hypothesis. *J Geophys Res* **96,** 16263–16274.

Hodges F. N. (1974) The solubility of H_2O in silicate melts. *Year Book Carnegie Inst Wash* **73,** 251–255.

Inoue T. (1994) Effect of water on melting phase relations and melt composition in the system Mg_2SiO_4-$MgSiO_3$-H_2O up to 15 GPa. *Phys Earth Planet Int* **85,** 237–263.

Iwamori H. (1998) Transportation of H_2O and melting in subduction zones. *Earth Planet Sci Lett* **160,** 65–80.

Jogoutz E., Palme H., Baddenhausen H., Blum K., Cendales M., Dreibus G., Wänke H. (1979) The abundances of major, minor and trace elements in the earth's mantle as derived from primitive ultramafic nodules. Proceedings 10th Lunar Science Conference. p. 2031–2050.

Kato T. and Kumazawa M. (1985) Effect of high pressure on the melting phase relations in the system Mg_2SiO_4-$MgSiO_3$ (I): Eutectic relations up to 7 GPa. *J. Phys. Earth.* **33,** 513–524.

Kato T., Ringwood A. E., and Irifune T. (1988a) Experimental determination of element partitioning between silicate perovskites, garnets and liquids: Constraints on early differentiation of the mantle. *Earth Planet Scie Lett* **89,** 123–145.

Kato T., Ringwood A. E., and Irifune T. (1988b) Constraints on element partition coefficients between $MgSiO_3$ perovskite and liquid determined by direct measurements. *Earth Planet Scie Lett* **90,** 65–68.

Kawamoto T. and Holloway J. R. (1997) Melting temperature and partial melt chemistry of H_2O-saturated mantle peridotites to 11 gigapascals. *Science* **276,** 240–243.

Kelemen P. B. (1995) Genesis of high Mg# andesites and the continental crust. *Contrib Mineral Petrol* **120,** 1–19.

Kennedy G. C., Wasserburg G. J., Heard H. C., and Newton R. C. (1962) The upper three phase region in the system SiO_2-H_2O. *Am J Sci* **260,** 501–521.

Kumazawa M. (1981) Origin of materials in the Earth's interior and their layered distribution. *J Mineral Petrol Econ Geol Special Issue* **3,** 239–247.

Kushiro I., Yoder Jr H. S., and Nishikawa M. (1968) Effect of water on the melting of enstatite. *Geol Soc Am Bull* **79,** 1685–1692.

Lesher C. E. and Walker D. (1988) Cumulate maturation and melt migration in a temperature gradient. *J Geophys Res* **93,** 10295–10311.

Luth R. W. (1993) Melting in the Mg_2SiO_4-H_2O system at 3 to 12 GPa. *Geophys Res Lett* **20,** 233–235.

Luth R. W. (1995) Is phase A relevant to the Earth's mantle? *Geochim Cosmochim Acta* **59,** 679–682.

Manning C. E. (1994) The solubility of quartz in H_2O in the lower crust and upper mantle. *Geochim Cosmochim Acta* **58,** 4831–4839.

McFalane E. A., Drake M. J., and Rubie D. C. (1994) Element partitioning between Mg-perovskite, magnesiowüstite, and silicate melt at conditions of the Earth's mantle. *Geochim Cosmochim Acta* **58,** 5161–5172.

Mibe K., Fujii T., and Yasuda A. (1997) Compositions of aqueous fluid coexisting with mantle minerals at high pressures: The role of water on the differentiation of the mantle (abstract). Terra Nova **9** (Suppl.), 483.

Mibe K., Fujii T., and Yasuda A. (1998) Connectivity of aqueous fluid in the Earth's upper mantle. *Geophys Res Lett* **25,** 1233–1236.

Mibe K., Fujii T., and Yasuda A. (1999) Control of the location of the volcanic front by aqueous fluid connectivity in the mantle wedge. *Nature* **401,** 259–262.

Mysen B. O. and Boettcher A. L. (1975) Melting of a hydrous mantle: I. Phase relations of natural peridotite at high pressures and temperatures with controlled activities of water, hydrogen, and carbon dioxide. *J Petrol* **16,** 520–548.

Mysen B. O. and Wheeler K. (2000) Alkali aluminosilicate-saturated aqueous fluids in the earth's upper mantle. *Geochim Cosmochim Acta* **64,** 4243–4256.

Nakamura Y. (1974a) The system SiO_2-H_2O-H_2 at 15 kbar. *Year Book Carnegie Inst Wash* **73,** 259–263.

Nakamura Y. and Kushiro I. (1974b) Composition of the gas phase in Mg_2SiO_4-SiO_2-H_2O at 15 kbar. *Year Book Carnegie Inst Wash* **73,** 255–258.

Ohtani E. (1985) The primordial terrestrial magma ocean and its implications for stratifications of the mantle. *Phys Earth Planet Int* **38,** 70–80.

Ohtani E. and Kumazawa M. (1981) Melting of forsterite Mg_2SiO_4 up to 15 GPa. *Phys Earth Planet Int* **27,** 32–38.

Ohtani E. and Ringwood A. E. (1984) Composition of the core, I. Solubility of oxygen in molten iron at high temperatures. *Earth Planet Scie Lett* **71,** 85–93.

Ohtani E., Kato T., and Sawamoto H. (1986) Melting of a model chondritic mantle to 20 GPa. *Nature* **322,** 352–353.

Pacalo R. E. G. and Gasparik T. (1990) Reversals of the orthoenstatite–clinoenstatite transition at high pressures and high temperatures. *J. Geophys. Res.* **95,** 15853–15858.

Palme H. and Nickel K. G. (1985) Ca/Al ratio and composition of the Earth's upper mantle. *Geochim. Cosmochim. Acta* **49,** 2123–2132.

Ringwood A. E. (1966) The chemical composition and origin of the Earth. In *Advances in Earth Science* (ed. P. M Hurley), pp. 287–356. Massachusetts Institute of Technology Press.

Ringwood A. E. (1977) Composition of the core and implications for origin of the earth. *Geochem J* **11,** 111–135.

Rudnick R. L. (1995) Making the continental crust. *Nature* **378,** 571–578.

Ryabchikov I. D., Schreyer W., and Abraham K. (1982) Compositions of aqueous fluid in equilibrium with pyroxenes and olivines at mantle pressures and temperatures. *Contrib Mineral Petrol* **79,** 80–84.

Schneider M. E. and Eggler D. H. (1986) Fluids in equilibrium with peridotite minerals: Implications for mantle metasomatism. *Geochim Cosmochim Acta* **50,** 711–724.

Stalder R. and Ulmer P. (2001) Phase relations of a serpentine composition between 5 and 14 GPa: Significance of clinohumite and phase E as water carriers into the transition zone. *Contrib Mineral Petrol* **140,** 670–679.

Stalder R., Ulmer P., Thompson A. B., and Günther D. (2001) High pressure fluids in the system MgO-SiO_2-H_2O under upper mantle conditions. *Contrib Mineral Petrol* **140,** 607–618.

Takahashi E. (1986) Melting of a dry peridotite KLB-1 up to 14 GPa: Implications on the origin of peridotic upper mantle. *J Geophys Res* **91,** 9367–9382.

Takei Y. and Shimizu I. (2001) Compositional dependence of dihedral angles in partially molten systems: Thermostatistical models. In Proceedings of the Deformation Mechanisms, Rheology and Tectonics Meeting, p. 160.

Tatsumi Y. (1989) Migration of fluid phases and genesis of basalt magmas in subduction zones. *J Geophys Res* **94,** 4697–4707.

Taylor S. R. (1967) The origin and growth of continents. *Tectonophysics* **4,** 17–34.

Taylor S. R. and McLennan S. M. (1985) *The Continental Crust: Its Composition and Evolution*. Blackwell Scientific Publications.

Walker D., Jurewicz S., and Watson E. B. (1988) Adcumulus dunite growth in a laboratory thermal gradient. *Contrib Mineral Petrol* **99,** 306–319.

Wasson J. T. and Kallemeyn G. W. (1988) Composition of chondrites. *Phil Trans R Soc Lond A* **325,** 535–544.

Watson E. B. and Brenan J. M. (1987) Fluids in the lithosphere. 1: Experimentally-determined wetting characteristics of CO_2-H_2O fluids and their implications for fluid transport, host-rock physical properties, and fluid inclusion formation. *Earth Planet Scie Lett* **85,** 497–515.

Watson E. B., Brenan J. M., and Baker D. R. (1990) Distribution of fluid in the continental mantle. *Continental Mantle*, Oxford University Press, Oxford.

Wiik B. (1956) The chemical composition of some stony meteorites. *Geochim Cosmochim Acta* **9,** 279–289.

Yagi T., Akaogi M., Shimomura O., Suzuki T., and Akimoto S.-I. (1987) In situ observation of the olivine–spinel phase transformation in Fe_2SiO_4 using synchrotron radiation. *J Geophys Res* **92,** 6207–6213.

Yamamoto K. and Akimoto S.-I. (1977) The system MgO-SiO_2-H_2O at high pressures and temperatures–stability field for hydroxyl–chondrodite and 10Å-phase. *Am J Sci* **277,** 288–312.

Yasuda A., Fujii T., and Kurita K. (1990) Melting relation of an anhydrous abyssal basalt at high pressure. In *Dynamic Processes of Material Transport and Transformation in the Earth's Interior* (ed. F Marumo), 327–337. Terrapub.

Zhang J. and Herzberg C. T. (1994) Melting experiments on anhydrous peridotite KLB-1 from 5.0 to 22.5 GPa. *J Geophys Res* **99,** 17729–17742.

Zhang J., Li B., Utsumi W., and Lieberman R. C. (1996) In situ X-ray observations of the coesite–stishovite phase transformation: Reversed phase boundary and kinetics. *Phys Chem Minerals* **23,** 1–10.

Zhang Y.-G. and Frantz J. D. (2000) Enstatite–forsterite–water equilibria at elevated temperatures and pressures. *Am. Mineral.* **85,** 918–925.